to appear in: Annals of the New York Academy of Sciences

Chaos in Cosmological Hamiltonians^a

HENRY E. KANDRUP b AND JOHN DRURY

Department of Astronomy, University of Florida, Gainesville, Florida 32611

This paper summarises a numerical investigation which aimed to identify and characterise regular and chaotic behaviour in time-dependent Hamiltonians $H(\mathbf{r}, \mathbf{p}, t) = \mathbf{p}^2/2 + V(\mathbf{r}, t)$, with $V = R(t)V_0(\mathbf{r})$ or $V = V_0[R(t)\mathbf{r}]$, where V_0 is a polynomial in x, y, and/or z and $R(t) \propto t^p$ is a time-dependent scale factor. When p is not too negative, one can distinguish between regular and chaotic behaviour by determining whether an orbit segment exhibits a sensitive dependence on initial conditions. However, chaotic segments in these potentials differ from chaotic segments in time-independent potentials in that a small initial perturbation will usually exhibit a sub- or super-exponential growth in time. Although not periodic, regular segments typically exhibit simpler shapes, topologies, and Fourier spectra than do chaotic segments. This distinction between regular and chaotic behaviour is not absolute since a single orbit segment can seemingly change from regular to chaotic and visa versa. All these observed phenomena can be understood in terms of a simple theoretical model.

INTRODUCTION

The past several decades have witnessed a growing recognition that chaotic behaviour is seemingly ubiquitous in Nature, and that chaos could play an important role in many problems of astronomical interest, extending from stellar pulsations to galactic dynamics (see. e.g., Ref. [1]). It thus seems natural to consider the possibility that chaos could play an important role in problems related to cosmology, large scale structure, and quantum field theory in the early Universe. However, cosmological problems lead to an important new ingredient, namely the expansion of the Universe, which implies, e.g., that, even if the system of interest is symplectic, the Hamiltonian H(t) generating the evolution will usually have an explicit systematic time dependence. The obvious question then is: what effects, if any, will this time dependence have on the possibility of chaotic behaviour?

One example of some interest is the gravitational N-body problem, as formulated for a large system of objects of comparable mass. In the context of isolated systems like individual galaxies, where the expansion of the Universe plays no role, the N-body problem is known to be chaotic in the sense that small initial perturbations in the locations of individual "particles" grow exponentially (see. e.g., Refs. [2-4] and references contained therein). However, despite some preliminary investigations [5] it is not yet clear whether

^a Some of the computations were facilitated by computer time made available through the Research Computing Initiative at the Northeast Regional Data Center (Florida) by arrangement with IBM.

^b Also with the Department of Physics and Institute for Fundamental Theory, University of Florida, Gainesville, Florida 32611.

this exponential instability persists for the cosmological N-body problem, as formulated in a comoving frame that expands with the Universe. Another cosmological example involving a time-dependent Hamiltonian is the problem of particle creation in the early Universe, e.g., in the context of the phenomenon of preheating, which leads to what Kofman, Linde & Starobinsky [6] have termed a "stochastic resonance."

But why might one expect that chaos will manifest itself differently in a cosmological context than for systems characterised by a time-independent H? For time-independent Hamiltonian systems, an orbit is usually said to be chaotic if and only if it has one or more positive Lyapunov exponents (see. e.g., Ref. [7]). However, these Lyapunov exponents can be defined in terms of the average properties of the stability matrix associated with an orbit, as evaluated along that orbit in an asymptotic $t \to \infty$ limit. Assuming canonical variables, the problem of stability, and hence the possibility of chaos, thus hinges on the properties of solutions to

$$\frac{d\delta Z^{i}}{dt} = \mathcal{J}^{ij} \frac{\partial^{2} H}{\partial Z^{j} \partial Z^{k}} \bigg|_{Z_{0}} \delta Z^{k} \equiv \Lambda^{i}_{k}(t) \delta Z^{k}, \tag{1}$$

where δZ^i denotes a perturbed phase space coordinate, \mathcal{J}^{ij} is the cosymplectic form [8], and $\Lambda^i_{k}(t)$ is a function of t because of its dependence on the unperturbed trajectory $Z_0^i(t)$. In particular, for a Hamiltonian

$$H = \frac{1}{2}\mathbf{p}^2 + V(\mathbf{r}),\tag{2}$$

the configuration space perturbation satisfies

$$\frac{d\delta r^a}{dt^2} = -\frac{\partial^2 V}{\partial r^a \partial r^b} \bigg|_{r_0(t)} \delta r^b.$$
(3)

If, e.g., the second derivative matrix $\partial^2 V/\partial r^a \partial r^b$ is constant and has at least one negative eidenvalue, there exist solutions that grow exponentially in time. If, however, that matrix acquires a secular time dependence this is no longer guaranteed to be true. For example, the one-dimensional equation

$$\frac{d^2\delta r}{dt^2} = \Omega^2(t)\delta r = \frac{\Omega_0^2}{t^2}\delta r \tag{4}$$

admits solutions which exhibit a power law growth. Just as an expanding Universe can convert an exponential Jeans instability into a milder power law instability [9], it might be expected to make chaotic orbits "less chaotic."

For time-independent Hamiltonian systems, sensitive dependence on initial conditions and the existence of one or more positive Lyapunov exponents is not the only way in which chaotic orbits differ from regular orbits. Regular and chaotic orbits also have very different Fourier spectra. Because regular orbits are multiply periodic, they will have computed spectra where (at least if one integrates long enough) most of the power is concentrated at or near a relatively small number of frequencies, whereas the spectra for chaotic orbits should exhibit substantially broader band power. (Strictly speaking, not every flow admitting one or more positive Lyapunov exponents must have nonzero power for a continuous range of frequencies, but one anticipates that, as a practical matter, positive Lyapunov exponents and broad band power go hand in hand [10].)

The situation is very different for Hamiltonian systems which manifest a systematic secular time-dependence. In this case, one anticipates generically that no orbit can be truly periodic, so that even spectra which one might wish to interpret as corresponding to "regular" orbit segments should have Fourier spectra with broad band power. This does not necessarily mean that an examination of the Fourier spectra cannot be used to distinguish between regular and chaotic behaviour. However, it *does* imply that any satisfactory discriminant based on an inspection of Fourier spectra must be more subtle than determining whether power is concentrated at or near a small number of frequencies.

The next section suggests a simple theoretical model based on a generalised Matthieu equation which can be used to make substantive predictions regarding the existence and manifestations of chaos in time-dependent Hamiltonian systems. This is followed by two sections which describe in detail a collection of experiments which were performed to test the predictions based on this model and the results of those experiments. A final section concludes by denumerating the principal conclusions.

THEORETICAL EXPECTATIONS

To make reasonable predictions regarding the behaviour of orbits in time-dependent Hamiltonian systems, including possible sensitive dependence on initial conditions, it is useful to understand precisely why chaotic behaviour can arise in time-independent Hamiltonian systems. For such systems, an exponentially sensitive dependence on initial conditions, as manifested by the existence of one or more positive Lyapunov exponents, is related to solutions to the linearised evolution equation (3) satisfied by a small initial δr^a , which can be interpreted as a time-dependent oscillator equation of the form

$$\frac{d^2\delta r^a}{dt^2} = -\Omega_{ab}^2(t)\delta r^b. \tag{5}$$

If the matrix Ω_{ab}^2 is constant in time and all its eigenvalues are nonnegative, solutions to this equation involve stable oscillations, so that a small initial perturbation cannot grow exponentially. Alternatively, if Ω_{ab}^2 is constant but has one or more negative eigenvalues, there do exist small perturbations that grow exponentially, which implies a sensitive dependence on initial conditions. However, this latter possibility does not seem very realistic: if there is always at least one negative eigenvalue, the potential V is not bounded from below!

The important point, therefore, is that instability is not necessarily associated simply with the fact that the second derivative matrix $\partial^2 V/\partial r^a \partial r^b$ has a negative eigenvalue. Indeed, many nonintegrable potentials that admits large amounts of chaos, including all the finite order truncations of the Toda potential [11], yield a second derivative matrix that is everywhere nonnegative. Rather, as has been discussed elsewhere [12-14] in the context of Maupertuis' Principle, where the flow associated with a time-independent H is reinterpreted as a geodesic flow on a curved manifold, chaos in time-independent Hamiltonian systems can be understood as resulting from a parametric instability.

The idea is very simple. Given a knowledge of the unperturbed orbit, $\mathbf{r}_0(t)$, one could diagonalise eq. (5) and then express the second derivative matrix in terms of its Fourier

transform to conclude that each eigenvector δr^A satisfies an equation of the form

$$\frac{d^2 \delta r^A}{dt^2} = -\left[\mathcal{C}_0^A + \sum_{\alpha} \mathcal{C}_\alpha^A \cos\left(\omega_\alpha t + \varphi_\alpha\right)\right] \delta r^A,\tag{6}$$

where, of course, the sum must be interpreted as a Stiltjes integral. The obvious point, then, is that, even if the coefficients \mathcal{C}^A_{α} are sufficiently small that the term in brackets, and hence the eigenvalues of the stability matrix, are always nonnegative, there is the possibility of resonant behaviour leading to solutions that grow exponentially in time. One simple example, corresponding to the case where there is only one nonzero frequency ω_{α} , is the Matthieu equation [15], which can be written in the form

$$\frac{d^2\xi}{dt^2} = -(A + B\cos 2t)\xi. \tag{7}$$

As is well known, a study of solutions to eq. (7) as a function of A and B reveals that the A-B plane divides naturally into distinct, well defined regions corresponding to stable and unstable motions. In the stable regions, solutions to eq. (7) are purely oscillatory; in the unstable regions they exhibit a systematic exponential growth, i.e., $|\xi(t)| \sim \exp(\chi t)$. The precise value of χ depends on A and B, so that, e.g., unstable values of A and B especially close to stable regions correspond to especially small (but still positive) values of χ . However, the fact that $\ln |\xi|$ grows linearly in time is robust. Allowing for generalisations of eq. (7) which incorporate one or more additional frequencies does not change the basic picture. In some cases, ξ is bounded but, for other choices of parameters, ξ grows in such fashion that $\ln |\xi|$ is reasonably well fit by a linear growth law.

The obvious question then is: how do things change if the Hamiltonian H acquires an explicit time dependence? Consider, e.g., the simplest possible time-dependence, where the potential is multiplied by an overall time-dependent factor, so that

$$H = \frac{1}{2}\mathbf{p}^2 + R(t)V(\mathbf{r}),\tag{8}$$

with R(t) a specified function of time. In this case, the natural analogue of eq. (7) becomes

$$\frac{d^2\xi}{dt^2} = -R(t)(A + B\cos 2t)\xi,\tag{9}$$

(or, perhaps, a generalisation thereof with $\cos 2t$ replaced by $\cos 2\tau(t)$). Even if R(t) evidence a systematic secular time-dependence, one can often make reasonable distinctions between solutions to eq. (9) that do and do not grow rapidly in time. However, in general the rapidly growing "unstable" solutions will not exhibit a purely exponential growth.

Consider, e.g., the case where $R(t) = R_0 t^p$, with p a real constant. Here trivial numerical computations reveal that, at least for values of p somewhat larger than p = -2, the evolution of ξ can be well understood in an adiabatic approximation. The factor $R \propto t^p$ in the potential implies that the instantaneous "natural" frequencies ω with which ξ grows or oscillates should scale as $R^{1/2}(t) \propto t^{p/2}$; but, in the adiabatic approximation this leads to a time dependence

$$\int dt \,\omega(t) \sim \int dt \,R^{1/2}(t) \sim t^{1+p/2}.\tag{10}$$

It follows that, for p > 0, unstable solutions correspond to superexponential growth, so that $\ln |\xi| \sim a + bt^q$, with $q = 1 + \frac{p}{2} > 1$. Alternatively, for $-2 , unstable solutions correspond to subexponential growth with <math>q = 1 + \frac{p}{2} < 1$. The adiabatic approximation fails for values of p that are too small, the special case p = -2 corresponding instead to solutions that exhibit a (possibly oscillatory) power law time dependence.

The other obvious point is that a single initial condition evolved with eq. (9) can exhibit transitions from stable to unstable motions and visa versa, this corresponding to transitions between regular and chaotic behaviour. Solutions to the ordinary time-independent Matthieu equation involve either stable or unstable motion, depending on the values of A and B, which do not change in time. However, incorporating a time dependence as in eq. (9) involves allowing for time-dependent "dressed" quantities $\hat{A} = t^{p/2}A$ and $\hat{B} = t^{p/2}B$. In the adiabatic approximation, the time dependence involves \hat{A} and \hat{B} evolving through a sequence of values corresponding to a line in the A - B plane. This line will in general intersect both stable and unstable regions, corresponding to intervals of both regular and chaotic motions.

The basic inference is that, for Hamiltonian systems of the form given by eq. (8) with $R \propto t^p$, power laws p > 0 yield small perturbations of "chaotic" orbit segments that exhibit superexponential growth, whereas power laws p < 0 yield small perturbations that exhibit subexponential or power law growth. For more complicated Hamiltonians, e.g., $H = \frac{1}{2}\mathbf{p}^2 + V[\mathbf{r}/R(t)]$, the simple scaling that leads to eq. (10) no longer holds. However, by analogy with the preceeding one would anticipate that if the characteristic size of the second derivative matrix $\frac{\partial^2 V(t)}{\partial r^a \partial r^b}$ is increasing systematically in time, small perturbations of chaotic orbits should grow faster than exponentially, whereas the growth should be slower than exponential if this matrix is decreasing systematically. The examples described in the following sections corroborate this physical expectation.

NUMERICAL EXPERIMENTS PERFORMED

The numerical experiments described here were performed for time-dependent extensions of the time-independent potential

$$V_0(x,y,z) = -(x^2 + y^2 + z^2) + \frac{1}{4}(x^2 + y^2 + z^2)^2 - \frac{1}{4}(ay^2z^2 + bz^2x^2 + cx^2y^2),$$
(11)

which is itself an obvious three-dimensional generalisation of the two-dimensional dihedral potential of Armbruster, Guckenheimer, & Kim [16] for specific choices of parameter values. The simplest extension, most easily compared with theory, involved introducing an overall multiplicative factor, setting

$$V(x, y, z, t) = R(t)V_0(x, y, z),$$
(12)

with $R(t) = t^p$. Another alternative involved mimicking the effects of comoving coordinates by setting

$$V(x, y, z, t) = V_0[R(t)x, R(t)y, R(t)z],$$
(13)

again with $R(t) = t^p$. Some computations focused on fully three-dimensional orbits. Others focused on two-dimensional orbits with $z = p_z = 0$. It was found that, at least in terms of

their sensitive dependence on initial conditions, two- and three-dimensional orbits behaved very similarly but that, in terms of possible shapes, three-dimensional orbits exhibited a richer phenomenology.

Ensembles of ~ 1000 initial conditions for use in two-dimensional simulations were generated by freezing the energy of the time-independent H at a fixed value E, setting x=0, uniformly sampling the energetically allowed regions of the $y-p_y$ plane, and then solving for $p_x(x,y,p_y,E)>0$. Initial conditions for fully three-dimensional simulations were generated by freezing the energy at E, setting x=z=0, uniformly sampling the allowed regions of the $y-p_y-p_z$ cube, and solving for $p_x(x,y,z,p_y,p_z,E)>0$. Each ensemble was evolved into the future for a time t=256 or longer, with the initial time t_0 chosen to vary between $t_0=1.0$ and $t_0=100$. A reasonably broad range of exponents p was considered. The simulations with the potential (12) allowed for -1.5 . Those with the potential (13) allowed for <math>-1 .

The evolution equations were integrated using a fourth order Runge-Kutta algorithm with fixed time step δt ranging between 10^{-3} and 10^{-4} . The integrator solved simultaneously for the evolution of a small, linearised perturbation, renormalised at fixed intervals $\Delta t = 1.0$, to obtain an estimate of the largest short time Lyapunov exponent (cf. Ref. [7]). When focusing on time-independent Hamiltonian systems, it is customary to record a running Lyapunov exponent that is a numerical approximation to the quantity

$$\chi(t) = \lim_{\delta Z(0) \to 0} \frac{1}{t} \ln \left[\frac{||\delta Z(t)||}{||\delta Z(0)||} \right], \tag{14}$$

with ||.|| the natural Euclidean norm, which converges towards the true Lyapunov exponent χ in a $t \to \infty$ limit. In the context of a time-dependent potential, it is more natural to record short time Lyapunov exponents (cf. Ref. [17]) $\chi(\Delta t_i)$ for each interval Δt , which, for an integration begun at time t = 0, are related to $\chi(t)$ by [18]

$$\chi(\Delta t_i) = \frac{\chi(t_i + \Delta t)(t_i + \Delta t) - \chi(t_i)t_i}{\Delta t}.$$
 (15)

Given such $\chi(\Delta t_i)$'s, the partial sums

$$\xi(t_i) = \frac{1}{\Delta t} \sum_{j=1}^{i-1} \chi(\Delta t_j) = \frac{1}{\Delta t} \ln \left[\frac{||\delta Z(t_i + t_0)||}{||\delta Z(t_0)|||} \right]$$
(16)

capture the net growth of the initial perturbation within a time t_i .

Plots of $\chi(\Delta t_i)$ and $\xi(t_i)$ for individual orbit segments were examined visually in an effort to identify clear distinctions between regular and chaotic behaviour. For those orbit segments deemed chaotic, $\xi(t_i)$ was fitted to a growth law

$$\xi = a + bt^q \tag{17}$$

to determine (1) whether such a fit was reasonable and (2) whether the best fit yielded superor sub-exponential growth. Orbital data $\mathbf{r}(t)$ and $\mathbf{p}(t)$, and the associated Fourier spectra, $|\mathbf{r}(\omega)|$ and $|\mathbf{p}(\omega)|$, were also inspected visually in a search for distinguishing features. One aim was to determine whether orbit segments deemed regular also had simpler topologies and/or simpler spectra than chaotic segments that manifested a sensitive dependence on initial conditions. The other was to search for evidence for abrupt transitions between chaotic and regular behaviour.

RESULTS OF THE EXPERIMENTS

For values of p that are not too negative, it is often possible to distinguish relatively clearly between regular segments, where $\chi(\Delta t_i)$ fluctuates around zero, and chaotic segments, where, if one averages over several time steps, $\chi(\Delta t_i)$ is usually larger than zero. This distinction becomes especially apparent if, for an ensemble of segments in the same potential with the same value of p, one computes $N[\xi(t_{fin})]$, the distribution of the final values of ξ . This $N[\xi(t_{fin})]$ often corresponds to a bimodal distribution and, even when one seems to see only a single population, tracking the form of the distribution as a function of p usually allows one to determine whether that population is regular or chaotic.

This is illustrated in FIGURE 1, which was generated from an ensemble of 1000 initial conditions with energy E = 1.0 and $z = p_z = 0$, evolved for the interval 10.0 < t < 0266.0 in the potential $V = V_0[R(t)\mathbf{r}]$ of eq. (13) with a=1. The six panels correspond to different values of p ranging from p = -0.6 to p = 0.45. It is clear that, for the timeindependent case with p=0.0, the distributions of ξ 's is bimodal, the peak near $\xi=0$ corresponding to regular segments, and the segments with larger values of ξ corresponding to chaotic orbits. (A longer time integration reveals that the segments with $20 < \xi < 60$ correspond to "sticky" orbits which, at early times, were trapped near regular islands by one or more cantori.) This bimodal behaviour persists for p > 0, although the relative abundance of "regular" segments increases rapidly with increasing p. Alternatively, the relative abundance of regular segments decreases very rapidly when p becomes negative so that, for p < 0.1 or so, a sample of 1000 initial conditions is too few to yield an appreciable number of regular segments. These changes in the relative abundance of regular and chaotic segments probably reflect the specific form of the time-independent potential $V_0(\mathbf{r})$. For example, p > 0 implies that the kinetic energy $K = \mathbf{v}^2/2$ increases, the potential energy $V = t^p V_0(x,y)$ decreases in magnitude, and the total energy $E = \mathbf{v}^2/2 + t^p V_0(x,y)$ exhibits a modest systematic increase, with the net result that the orbits tend to evolve in a regular or near-regular fashion in the "trough" of the dihedral potential V(t).

Another generic feature, also apparent in FIGURE 1, is that, even though increasing p implies fewer chaotic segments, those segments that remain chaotic tend to be more unstable in the sense that the final $\xi(t_{fin})$ is larger. In part, this trend reflects the fact that, overall, the values of $\chi(\Delta t_i)$ tend to be larger for larger values of p. However, this trend also reflects the fact that, as expected, p > 0 yields perturbations that exhibit superexponential growth whereas p < 0 yields subexponential growth. For fixed sets of initial conditions, this latter assertion was confirmed for each value of p by (1) identifying a minimum value of ξ that (seemingly) represents a sufficient criterion for chaotic behaviour, (2) fitting the computed $\xi(t_i)$ for each chaotic segment to the power law (17), and (3) determining a mean slope for all the chaotic segments with given p. The results are exhibited in FIGURE 2 (a), where the error bars reflect the effects of reasonable variations in the value ξ_{min} used to identify chaotic behaviour.

FIGURE 2 agrees with predictions in the sense that p > 0 and p < 0 yield, respectively, super- and sub-exponential growth. However, there is one new, not completely expected feature, namely that q is not a monotonic function of p. In particular, there appears to be a range of values of p, say -0.25 where, as probed by the aforementioned diagnostic, the growth of a small initial perturbation is weaker than for both somewhat smaller and somewhat larger values of <math>p. Given this behaviour, it is especially important to check whether the predicted behaviour for the simpler potential $V = t^p V_0(\mathbf{r})$ is confirmed by experiments. FIGURE 2 (b), which presents the analogue of FIGURE 2 (a) for the same set of initial conditions now evolved in the potential (12), indicates that, overall, the agreement between theory and experiment is quite good, although some systematic differences are seen for p > 0. Note that the larger error bars for especially large and small p reflect the fact that, for these values of p, most of the orbits seem regular or near-regular, with very small values of $\chi(\Delta t_i)$ and $\xi(t_i)$.

A third general feature, also apparent from FIGURE 1, is that, for p's somewhat larger than zero, a larger fraction of the segments have values of ξ well separated from both the low and high ξ peaks than is the case for p=0. In most cases, these intermediate values appear to correspond to segments which change from chaotic to regular or, in some cases, from regular to chaotic. That this is the case is easily seen by computing either $\chi(\Delta t_i)$, which can exhibit abrupt systematic increases and decreases, or $\xi(t_i)$, which can exhibit a nearly stepwise growth. Two examples of this behaviour are provided in FIGURE 3, both corresponding to segments computed with p=0.5. The top two panels correspond to an orbit segment which makes an abrupt transition from chaotic to regular behaviour at $t \sim 160$; the lower panels correspond to a segment which exhibits a more erratic behaviour early on. It should also be evident that, during the chaotic phases, $\chi(\Delta t_i)$ is evidencing a systematic increase, so that $\xi(t_i)$ grows faster than linearly in time, this corresponding to a perturbation that evolves superexponentially.

Inspection of individual orbit segments also reveals that segments which are chaotic in the sense that they exhibit a sensitive dependence on initial conditions tend to be manifestly more irregular in visual appearance. In particular, regular segments typically have identifiable shapes and topologies which persist for relatively long periods of time, even as the orbital energy changes by an order of magnitude or more. Pieces of two representative regular orbits evolved it the potential (13) with a=1 and, respectively, p=0.3 and p=0.5, are exhibited in the top four panels of FIGURES 4 and 5. Viewed over relatively short intervals $\Delta t < 50$ or so, the first segment closely resembles a loop orbit in a time-independent potential. If, however, the orbit is tracked over longer intervals, one sees significant changes as the "radius" of the loop slowly decreases. The second segment, corresponding to the orbit used to generate FIGURE 3 (a) and (b), exhibits more distinct variability than the loop orbit, but it is evident once again that the overall shape and topology are robust.

These regularities imply that, even though regular segments are not periodic, their Fourier spectra are distinctly different, and simpler, than the spectra for chaotic segments. For example, like true loop orbits in a time-independent potential, regular segments that look loopy are characterised by spectra $|x(\omega)|$ and $|y(\omega)|$ which are very similar in amplitude and shape. Moreover, in many cases the overall form of the spectrum can be interpreted

as involving one or more peak frequencies ω whose values exhibit a systematic drift over the course of time. This is particularly evident in the final two panels of FIGURE 4, which exhibit $|x(\omega)|$ and $|y(\omega)|$ for the loopy regular orbit. At early times, when the orbit rotates relatively slowly, the power for both $|x(\omega)|$ and $|y(\omega)|$ is concentrated at relatively low values of ω but, as time elapses and the orbit begins to rotate more rapidly, power slides up to high values of ω . The composite spectra in FIGURES 4 (e) and (f) can be understood, at least approximately, as representing the time integral of a set of narrow peaks which, as time elapses, move systematically towards higher frequency.

CONCLUSIONS

This paper summarised a numerical investigation which focused on identifying meaningful definitions of regular and chaotic behaviour in time-dependent Hamiltonian systems of the type that one might expect to encounter in a cosmological setting. Especial attention focused on two- and three-dimensional Hamiltonians of the form $H(\mathbf{r}, \mathbf{p}, t) = \mathbf{p}^2/2 + V(\mathbf{r}, t)$, with $V = R(t)V_0(\mathbf{r})$ or $V = V_0[R(t)\mathbf{r}]$, where V_0 is a polynomial in x, y, and z and $R(t) \propto t^p$ represents a time-dependent scale factor. When p is not too negative, one can distinguish between regular and chaotic behaviour by determining whether, over the time interval in question, an orbit segment exhibits a sensitive dependence on initial conditions. However, the time-dependence of H complicates the physics in several important ways.

- 1. A single orbit can exhibit intermittent behaviour, changing from chaotic to regular and/or visa versa.
- 2. A small perturbation of a chaotic segment will not in general exhibit an average exponential growth. Rather, a computation of suitably defined short time Lyapunov exponents shows that the phase space perturbation δZ^i is often well fit by a growth law $\ln |\delta Z(t)| = a + bt^q$, with q > 1 for p > 0 and q < 1 for p < 0. An expanding Universe makes the effects of chaos milder; a contracting Universe makes them stronger.
- 3. Regular segments are not periodic and, as such, do not have sharply peaked Fourier spectra. However, the topology of regular segments is robust, so that, e.g., a loop orbit continues to look loopy even as $|\mathbf{r}|$ and $R(t)|\mathbf{r}|$ grow or shrink systematically. Moreover, the spectrum of a regular segment is simpler than that for a chaotic segment since, in many cases, the regular segment can be approximated as a sum of a few contributions of the form $Z(t) \sim Z(0) \exp[i\Omega(t)t]$, where $\Omega(t)$ exhibits a simple secular variation.

All these observed phenomena can be understood in terms of a simple theoretical model based on a time-dependent generalisation of the Matthieu equation.

ACKNOWLEDGMENTS

Work on this manuscript was completed while HEK was a visitor at the Aspen Center for Physics, the hospitality of which is acknowledged gratefully.

- 1. BUCHLER, J. R., S. L. GOTTESMAN, J. H. HUNTER & H. E. KANDRUP, 1998. Nonlinear Dynamics and Chaos in Astrophysics. New York Academy of Sciences, New York, in press.
- 2. KANDRUP, H. E. & H. SMITH, 1991. Astrophys. J. **374**: 255.
- 3. GOODMAN, J., D. HEGGIE & P. HUT, 1993. Astrophys J. **415**: 715.
- 4. KANDRUP, H. E., M. E. MAHON & H. SMITH, 1994. Astrophys. J. 428: 458.
- 5. MELOTT, A. 1998. private communication.
- 6. KOFMAN, L., A. LINDE & A. A. STAROBINSKY, 1994. Phys. Rev. Lett. **73**: 3195.
- 7. LICHTENBERG, A. J. & M. A. LIEBERMAN, 1992. Regular and Chaotic Dynamics. Springer-Verlag. Berlin.
- 8. ARNOLD, V. I. 1989. Mathematical Methods of Classical Mechanics. Springer-Verlag. Heidelberg.
- 9. PEEBLES, P. J. E. 1993. Principles of Physical Cosmology. Princeton University Press. Princeton.
- 10. TABOR, M. 1989. Chaos and Nonintegrability in Nonlinear Dynamics. Wiley. New York.
- 11. TODA, M. 1967. J. Phys. Soc. Japan 22: 431.
- 12. PETTINI, M. 1993. Phys. Rev. E 47: 828.
- 13. CERRUTI-SOLA, M. & M. PETTINI, 1995. Phys. Rev. E 53: 179.
- 14. KANDRUP, H. E. 1997. Phys. Rev. E. 56: 2722.
- 15. WHITTAKER, E. T. & G. H. WATSON, 1965. A Course of Modern Analysis. Cambridge University Press. Cambridge.
- 16. ARMBRUSTER, D., J. GUCKENHEIMER & S. KIM, 1989. Phys. Rev. Lett. A **140**: 416.
- 17. GRASSBERGER, P., R. BADII & A. POLITI, 1988. J. Stat. Phys. 51: 135.
- 18. KANDRUP, H. E. & M. E. MAHON, 1994. Astron. Astrophys. 290: 762.

- FIGS. 1 The distribution $N[\xi(t_{fin})]$, with ξ defined as in eq. (16), generated from an ensemble of initial conditions E = 1.0 and $z = p_z = 0$ evolved for the interval 10 < t < 266 in the potential (13) with a = 1.0 and variable p. (a) p = -0.6. (b) p = -0.1. (c) p = -0.05. (d) p = 0.0. (e) p = 0.2. (f) p = 0.45.
- FIGS. 2 (a) The mean slope q for chaotic segments generated as in FIG. 1, plotted as a function of p. (b) The analogue of (a) for chaotic segments generated in the potential (12), again with a=1.0 and variable p.
- FIGS. 3 (a) and (b) The short time Lyapunov exponent $\chi(\Delta t_i)$ and the cumulative $\xi(t_i)$ computed for one orbit with initial energy E=1.0 and $z=p_z=0$ evolved for the interval 10 < t < 266 in the potential (13) with p=0.5. (c) and (d) The same quantities for another orbit, again with E=1.0 and $z=p_z=0$, evolved for the same interval in the same potential.
- FIGS. 4 Segments of a single trajectory with E=1.0 and $z=p_z=0$ evolved with p=0.3 in the potential (13) for the interval 10 < t < 266, along with the total power spectra, $|x(\omega)|$ and $|y(\omega)|$. (a) 0 < t < 32. (b) 64 < t < 96. (c) 128 < t < 160. (d) 192 < t < 224. (e) $|x(\omega)|$. (f) $|y(\omega)|$.
- FIGS. 5 The analogue of FIG. 4 for another orbit with E = 1.0 and $z = p_z = 0$, now evolved with p = 0.5.

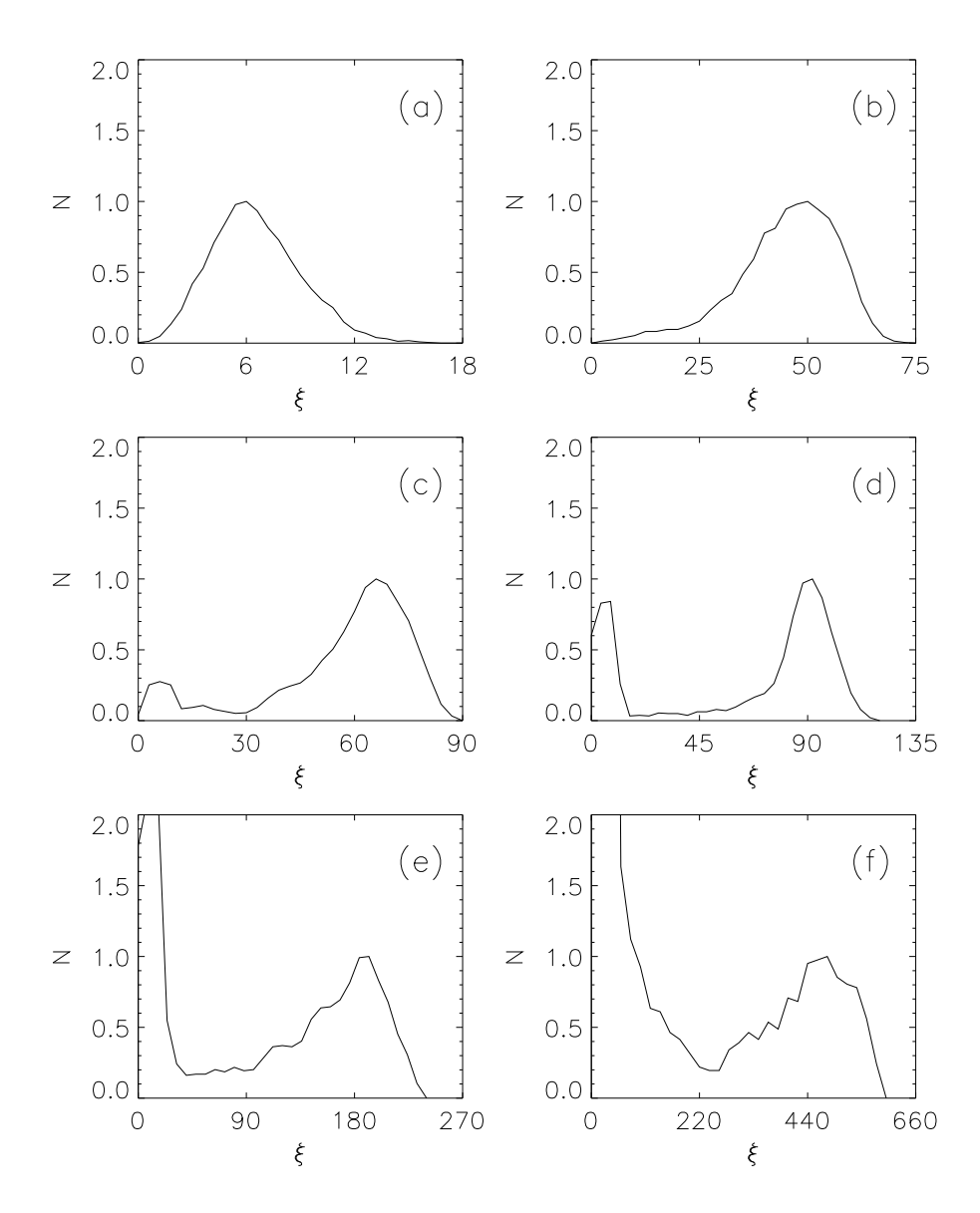


Figure 1.

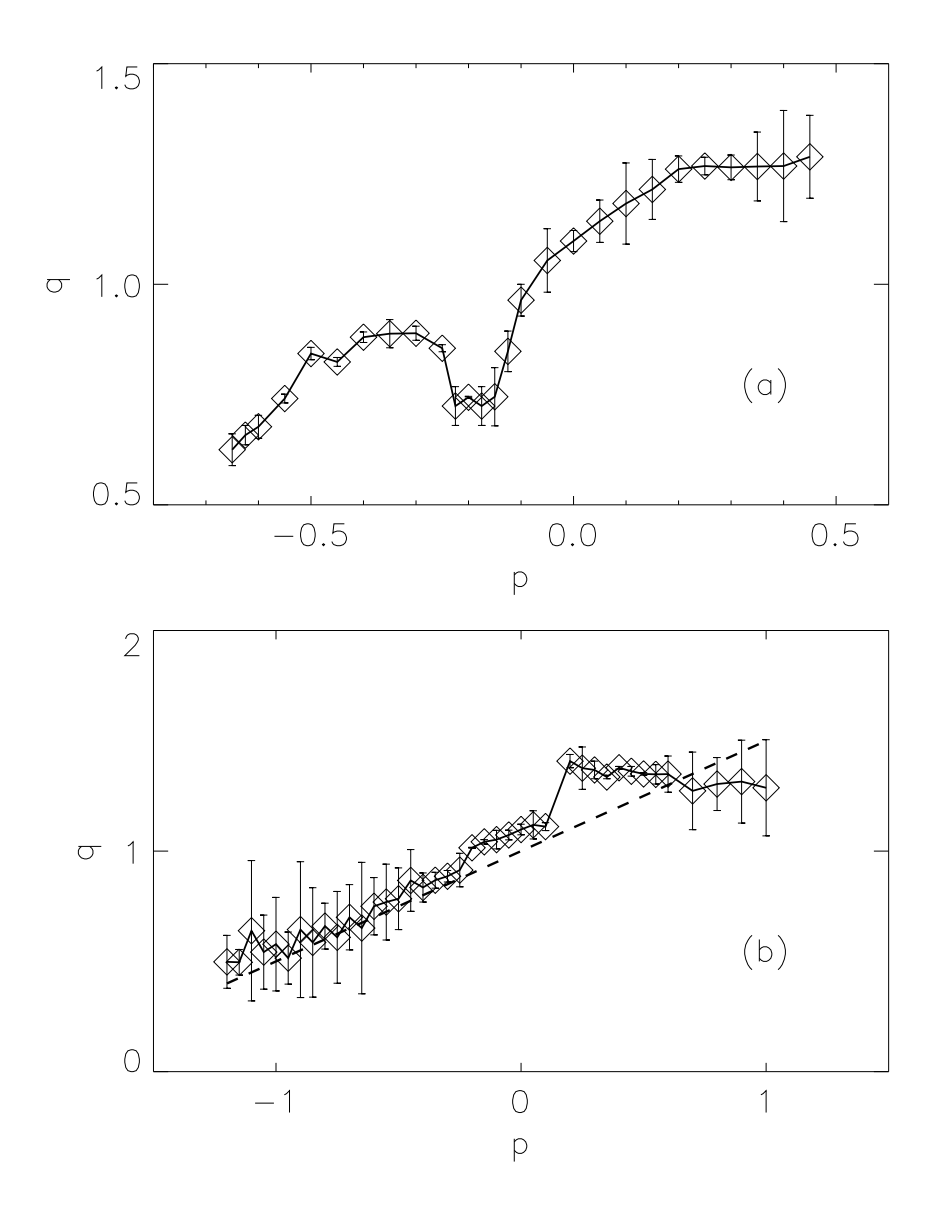


Figure 2.

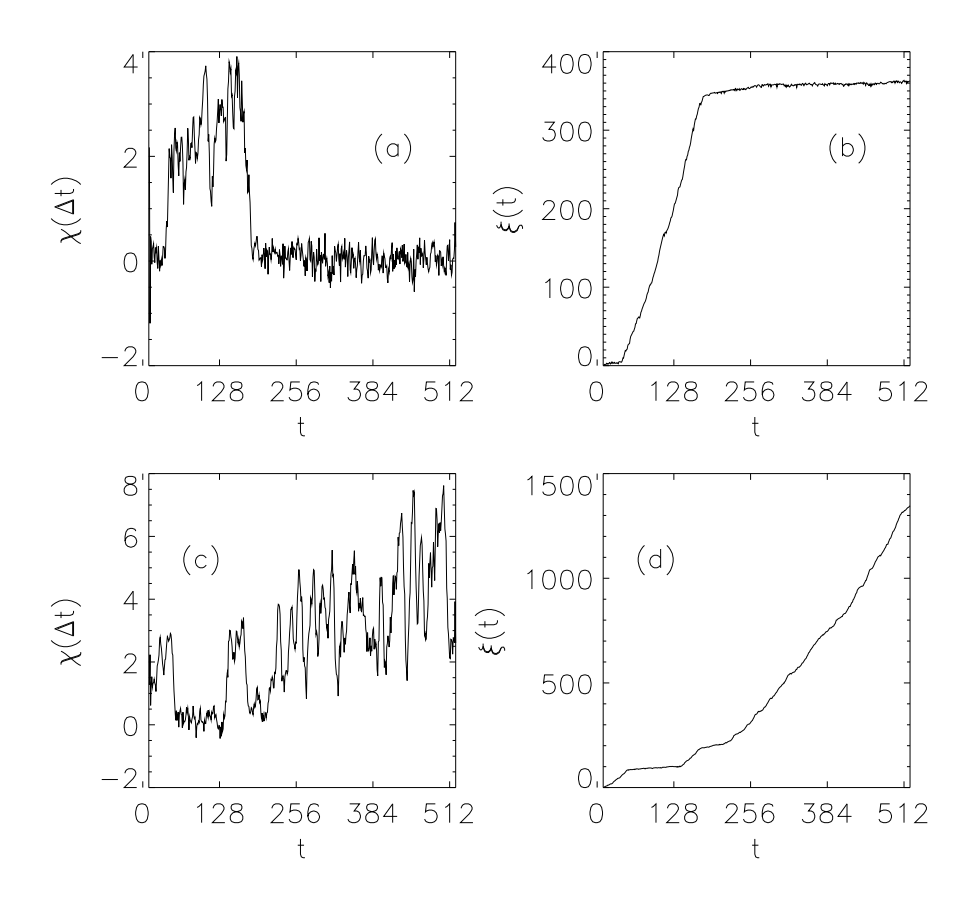


Figure 3.

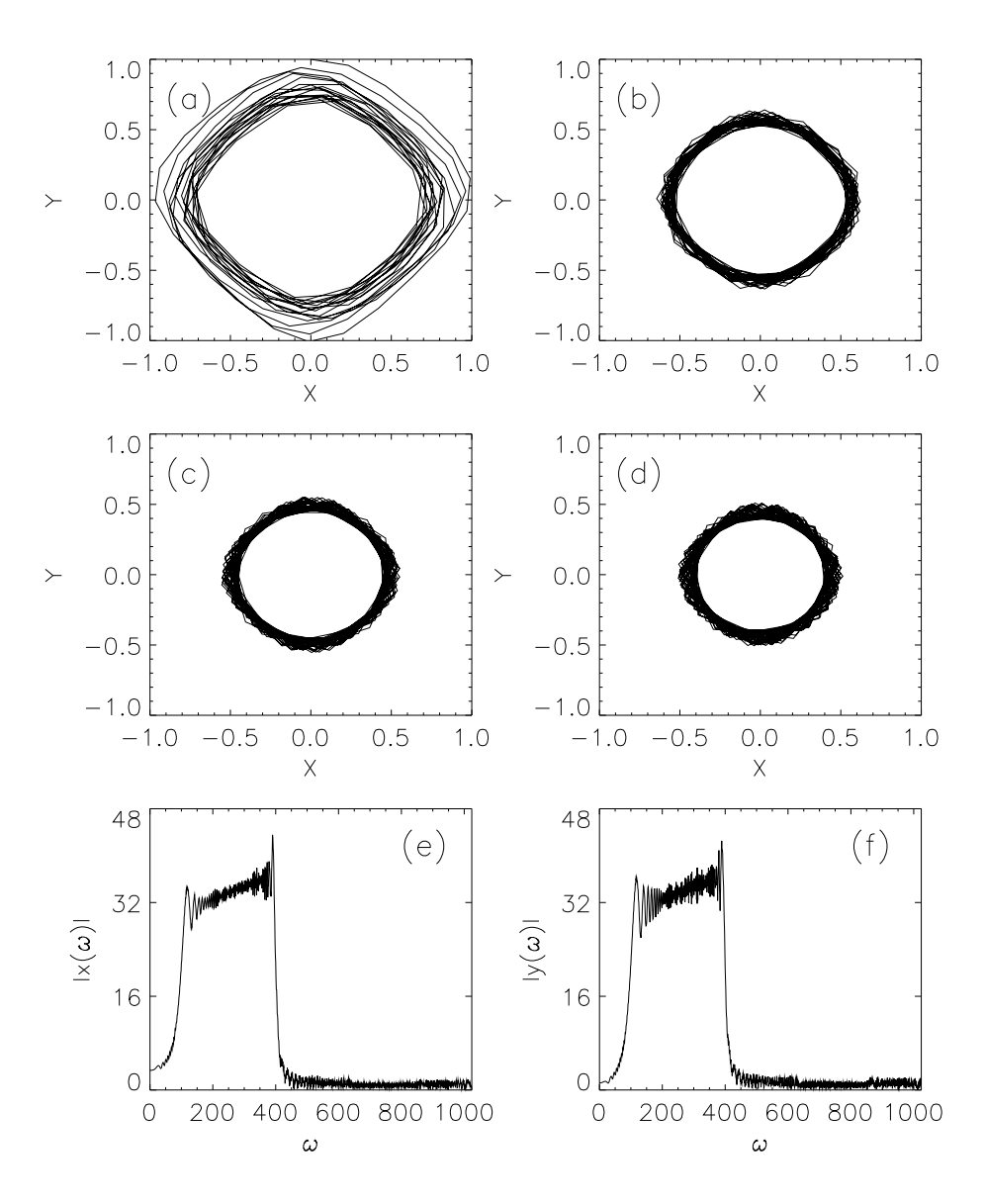


Figure 4.

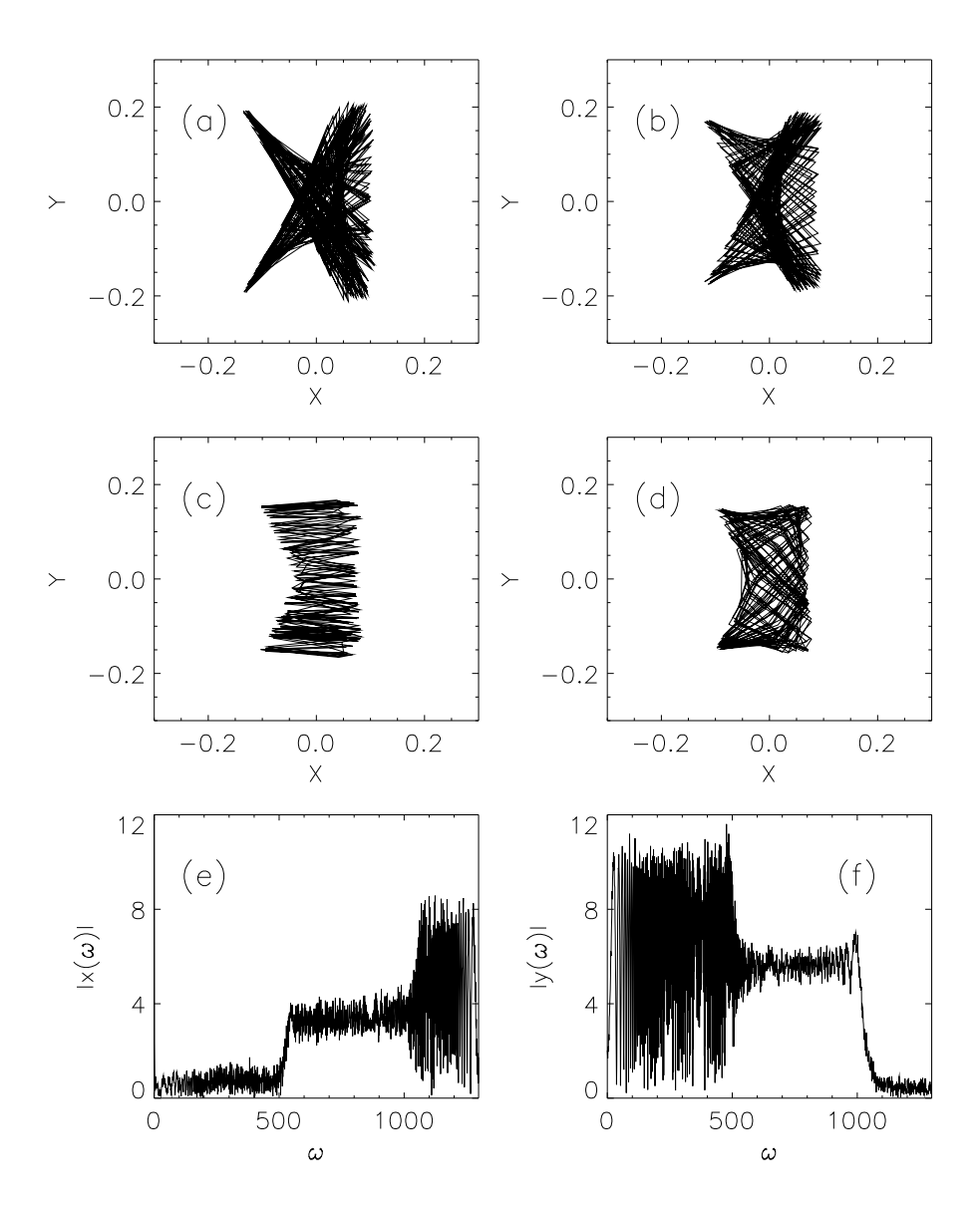


Figure 5.